Received: 9 December 2021 | Accepted: 11 December 2021

DOI: 10.1111/mmi.14864

RESEARCH ARTICLE

WILEY

Impairment of lysosomal function by *Clostridioides difficile* TcdB

Carmen Klepka[1] | Moritz Sandmann[1] | Helma Tatge[1] | Matthew Mangan[2,3] | Annabel Arens[1] | Daniel Henkel[1] | Ralf Gerhard[1]

[1]Institute of Toxicology, Hannover Medical School, Hannover, Germany

[2]Institute of Innate Immunology, Biomedical Center, University of Bonn, Bonn, Germany

[3]German Center for Neurodegenerative Diseases, Bonn, Germany

Correspondence
Ralf Gerhard, Institute of Toxicology, Hannover Medical School, Carl-Neuberg-Str. 1, 30625 Hannover, Germany.
Email: gerhard.ralf@mh-hannover.de

Funding information
Niedersächsisches Ministerium für Wissenschaft und Kultur, Grant/Award Number: VWZN3380; Deutsche Forschungsgemeinschaft, Grant/Award Number: GE1017/5-1 and GE1017/6-1

Abstract

TcdB is a potent cytotoxin produced by pathogenic *Clostridioides difficile* that inhibits Rho GTPases by mono-glucosylation. TcdB enters cells via receptor-mediated endocytosis. The pathogenic glucosyltransferase domain (GTD) egresses endosomes by pH-mediated conformational changes, and is subsequently released in an autoproteolytic manner. We here investigated the uptake, localization and degradation of TcdB. TcdB colocalized with lysosomal marker protein LAMP1, verifying the endosomal-lysosomal route of the toxin. In pulse assays endocytosed TcdB declined to a limit of detection within 2 hr, whereas the released GTD accumulated for up to 8 hr. We observed that autoproteolytic deficient TcdB NXN C698S was degraded significantly faster than wildtype TcdB, suggesting interference of TcdB with lysosomal degradation process. In fact, TcdB reduced lysosomal degradation of endosome cargo as tested with DQ-Green BSA. Lysosomal dysfunction was accompanied by perinuclear accumulation of LAMP1 and a weaker detection in immunoblots. Galectin-8 or galectin-3 was not recruited to lysosomes speaking against lysosome membrane damage. Changes in the autophagosomal marker LC3B suggested additional indirect effect of lysosomal dysfunction on the autophagic flux. In contrast to necrotic signaling induced in by TcdB, lysosomal dysfunction was not abolished by calcium channel blocker nifedipin, indicating separate cytopathogenic effects induced by TcdB during endo-lysosomal trafficking.

KEYWORDS
autophagic flux, *Clostridioides difficile* Toxin B, DQ-BSA assay, lysosome inhibition

1 | INTRODUCTION

One of the most common threats in nosocomial infections is the *Clostridioides difficile* associated disease and the more severe forms of *C. difficile* infections with clinical manifestations of pseudomembranous colitis and toxic megacolon. The urge for new therapy strategies rises since resistance of *C. difficile* against antibiotics increases. The two exotoxins TcdA and TcdB of *C. difficile* are promising therapeutic targets since both toxins represent the main pathogenicity factors, capable of inducing all clinical symptoms associated with *C. difficile*-associated disease. The search for neutralizing antibodies as well as for small compounds that reduce pathogenic effects of both toxins requires knowledge about structure-function relationship, molecular mode of action, and of the intracellular fate of toxins. So far, there is only one therapeutic antibody approved for treatment of *C. difficile* infections, which specifically neutralizes

TcdB (Wilcox et al., 2017). The disadvantage of antibodies is that they are powerless once the toxins have already entered cells. So far, there is only little knowledge about TcdB or related toxins regarding their intracellular persistence and degradation. Like most large protein toxins, TcdB and the homologous TcdA enter their target cells by receptor-mediated endocytosis. For TcdB three different binding proteins have been described, which are chondroitin sulfate proteoglycan-4 (CSPG4), Wnt-receptors frizzled-1,2,7, and poliovirus like protein-3/nectin-3 (PVRL3) that contribute to endocytotic uptake or TcdB effects (LaFrance et al., 2015; Tao et al., 2016; Yuan et al., 2015). Specifically acidification of the late endosomes to intravesicular pH <6 triggers conformational changes in TcdA and TcdB, allowing them to insert into the vesicular membrane and to deliver the pathogenic N-terminal glucosyltransferase domain into the cytosol (Jank & Aktories, 2008; Jank et al., 2015). Intracellular inositol hexakisphosphate ($InsP_6$) allosterically activates the toxin inherent cysteine protease domain upstream of the GTD, which releases the pathogenic GTD into the cytosol (Egerer et al., 2007; Jank & Aktories, 2008; Jank et al., 2015). Within the cytosol, the GTD catalyzes mono-glucosylation of the Rho GTPases, mainly Rho, Rac, and Cdc42, but also of other members of the Rho subfamily (Just et al., 1995; Zeiser et al., 2013). Although Rho glucosylation is considered to be the main pathogenic event (Bilverstone et al., 2020), glucosyltransferase-independent effects have also been attributed to the cytotoxic effect of TcdB (Farrow et al., 2013, 2020; Wohlan et al., 2014). The molecular mode of action for this early induced cell death is not known. It requires high toxin concentrations (Chumbler et al., 2012; Wohlan et al., 2014), rapid and sufficient uptake as well as signaling competent Rac1 (Beer et al., 2018a), and is not restricted to a specific receptor (Henkel et al., 2020). PVRL3 was reported to be essential for mediating cytotoxic effect (LaFrance et al., 2015), but depletion of CSPG4 could also prevent cytotoxic effect of TcdB (Henkel et al., 2020; Yuan et al., 2015). By investigating the intracellular route and degradation of TcdB we observed a delayed degradation of the toxin, suggesting a decrease in lysosomal degradation capacity in toxin-treated cells. This effect was independent of the glucosyltransferase activity and is also independent of the necrotic calcium signaling that triggers early cell death.

2 | RESULTS

2.1 | Intracellular translocation and degradation of the GTD

TcdB enters cells by receptor-mediated endocytosis. Acidification of late endosomes to a pH-value below 6.0 results in conformational changes of TcdB associated with passing the N-terminal GTD through the endosomal membrane, putatively by a pore formed by the trunk of the toxin (Barth et al., 2001; Giesemann et al., 2006; Orrell et al., 2017, 2020). Cytosolic $InsP_6$ activates the autoproteolytic release of the GTD by the adjacent cysteine protease domain. Since the time course of intracellular delivery of the GTD was unknown, we measured accumulation of the GTD within the cytosol of HEp-2 cells. To selectively follow full length TcdB as well as the cleaved GTD, we generated recombinant TcdB with a 3 × flag/myc-tag fused to the C-terminal end of the GTD between amino acid residues E540 and G541, directly upstream of the autoproteolytic cleavage site which is L543 (Figure 1a). The flag/myc-tagged TcdB ($TcdB^{fm}$) enabled us to detect full length toxins as well as cleaved GTDs with identical stoichiometric antibody ratio. This is also an advantage when chimeric toxins were used by exploiting a single system for standardized intracellular delivery of different GTD. In a cell rounding assay $TcdB^{fm}$ from reference strain VPI10463, clade 1, (termed $TcdB1^{fm}$-TcdB when compared with other chimeras) or of endemic strain R20291, clade 2, ($TcdB2^{fm}$-TcdB) were compared with recombinant wildtype TcdB from strain VPI10463 (Figure 1b). We found that the intramolecular flag/myc-tag did not negatively affect the biological function of TcdB, but instead significantly increased potency compared to non-tagged toxin. We assume that insertion of the flag-tag facilitates endosomal egress and autoproteolytic cleavage of the GTD resulting in more efficient intracellular release. Comparative in-vitro-cleavage of TcdB and $TcdB^{fm}$ supports this assumption as shown in Figure S1. Other characteristics such as more flexibility, facilitated membrane translocation or different pH-dependent conformational changes might also contribute to this observation. Wildtype TcdB2 (*C. difficile* strain R20291) is known to be less potent than TcdB1 (*C. difficile* strain VPI10463) because of lacking interaction with TcdB receptors frizzled 1,2,7 as recently reported (Henkel et al., 2020; Tao et al., 2016). After excluding a negative effect of flag/myc-tag on the function of TcdB we continued our experiments using the glucosyltransferase (GT)-deficient mutant D286/288N of $TcdB^{fm}$ ($TcdB^{fm}$ NXN). The use of GT-deficient TcdB avoids possible secondary effects on uptake or degradation of toxins that might be caused by Rho-inhibition. Furthermore, it allows localization of intracellular toxin by microscopy in cells with unchanged morphology.

We first followed accumulation of the released GTD within the cytosol of HEp-2 cells by immunoblot assays. We found that the majority of full length TcdB was endocytosed within 2 hr and that only residual holo-TcdB still bound to the cell surface or to petri dish, which did not change over observed period of 8 hr. We also found that TcdB bound to the extracellular surface of cells can artificially release the GTD when cells were lysed in NP-40 buffer. Thus, to avoid any cross contamination of the cytosolic fraction by extracellular bound GTD we harvested cells by mild trypsinization, which removed all extracellular bound toxin or toxin fragments (Figure 1c). Interestingly, although detection of full length by immunoblot decreased within 2 hr, the amount of intracellular GTD increased for a period of up to 8 hr after toxin uptake. This delay was true for the GTD from TcdB1 ($TcdB1^{fm}$-TcdB) as well as from TcdB2 ($TcdB2^{fm}$-TcdB) delivered by the trunk of TcdB VPI10463. 4–8 hr after toxin uptake into HEp-2 cells a maximum level of intracellular GTD was detected in immunoblots (Figure 1d,e). According to peak value and time, the GTD2 (from TcdB2) was delivered less efficiently by the trunk of TcdB1 than GTD1 from TcdB1, although differences were

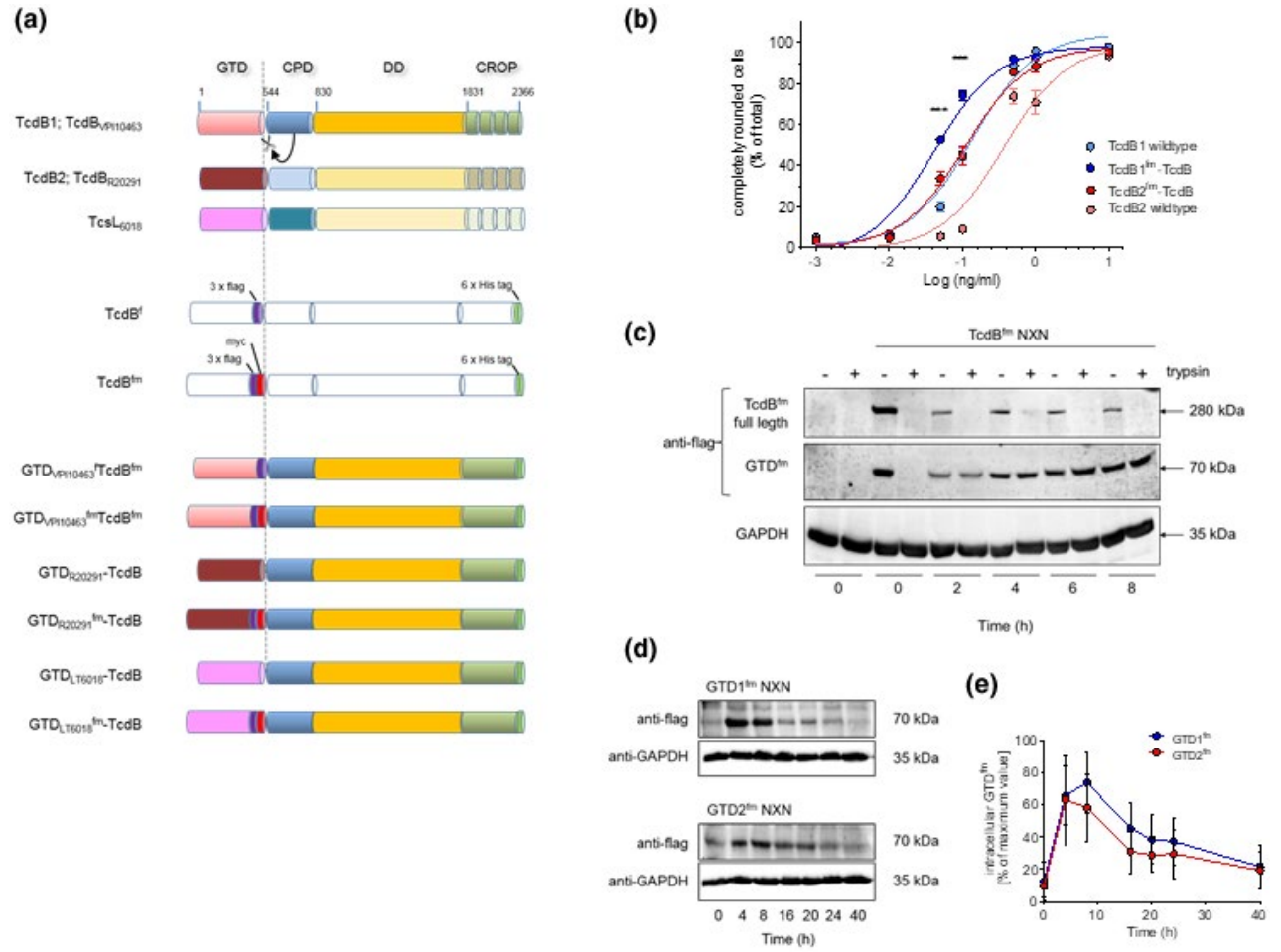

FIGURE 1 Intracellular accumulation of the GTD. (a) Schematic of TcdB showing the N-terminal glucosyltransferase domain (GTD), the cysteine protease domain (CPD), the delivery domain (DD), and the combined repetitive oligopeptides (CROP). At the C-terminal end of the GTD directly upstream of the cleavage site a 3 × flag tag and a myc-tag was inserted to detect intracellular delivery of the GTD. The recombinant chimeras of TcdB were generated to deliver the GTD of TcdB$_{R20291}$ (GTD$_{R20291}$-TcdB) and TcsL$_{6018}$ (GTD$_{LT6018}$-TcdB) into cells by standardized uptake. (b) Concentration-dependent cell rounding assay to measure functionality of flag/myc-tagged toxins after 4 hr treatment with indicated toxin. TcdB1^{FM}-TcdB (dark blue) was significantly more potent than untagged TcdB (light blue) (***$p < .0001$). The 3 × flag/myc-tag did not reduce potency of TcdB (TcdB^{fm}) or of the chimeric TcdB2^{fm}-TcdB. Shown are means ± SE, $n = 6$. (c) Immunoblot shows cell bound TcdB^{FM} NXN at time point 0 and the increase in intracellular GTD^{fm} over a time period of 8 hr. Extracellular bound TcdB^{fm} NXN was removed by limited trypsin digestion to specifically detect intracellular GTD^{fm} NXN. (d) Representative immunoblots showing intracellular 70 kDa GTD^{fm} NXN of TcdB1 (upper panel) and TcdB2 (lower panel) delivered in a pulse assay over a time period of 40 hr. GAPDH served as loading control. (e) Densitometrical evaluation of 6–8 independent immunoblots experiments as shown in (d). Shown are means ± *SD*, $n = 16$

not found to be significant. The majority of intracellular GTD was degraded within the next 16 hr and to a limit of detection 40 hr after toxin addition.

2.2 | Endocytosis and degradation of TcdB

To estimate the endosomal uptake and lysosomal degradation of TcdB we measured full-length TcdB in whole cell lysate by immunoblot analysis using affinity purified polyclonal rabbit anti-TcdB IgG. Extracellular bound TcdB^{fm} NXN was endocytosed and degraded in HEp-2 cells within 4 hr (Figure 2a). We used the non-cleavable mutant TcdB^{fm} NXN C698S in parallel as a control for complete lysosomal degradation of the toxin, since the GTD is not cleaved off and terminates with the rest of the toxin. To our surprise, the non-cleavable holo-TcdB was degraded much faster than cleavable TcdB possessing intact cysteine protease activity. The densitometrical evaluation in Figure 2b shows a time course of 3–8 independent experiments. There is a significant difference in clearance of TcdB within the first 90 min of toxin uptake. The observed difference was also found for GT-proficient TcdB that glucosylates Rho-GTPases which proves that this effect was not based on mutation of the DxD-motif (D286/288N; NXN) (Figure 2c). At a representative time point (30 min), flag/myc-tagged wildtype and the GT-deficient TcdB (TcdB^{fm}, TcdB^{fm} NXN) were compared with their non-cleavable counterparts (TcdB^{fm}

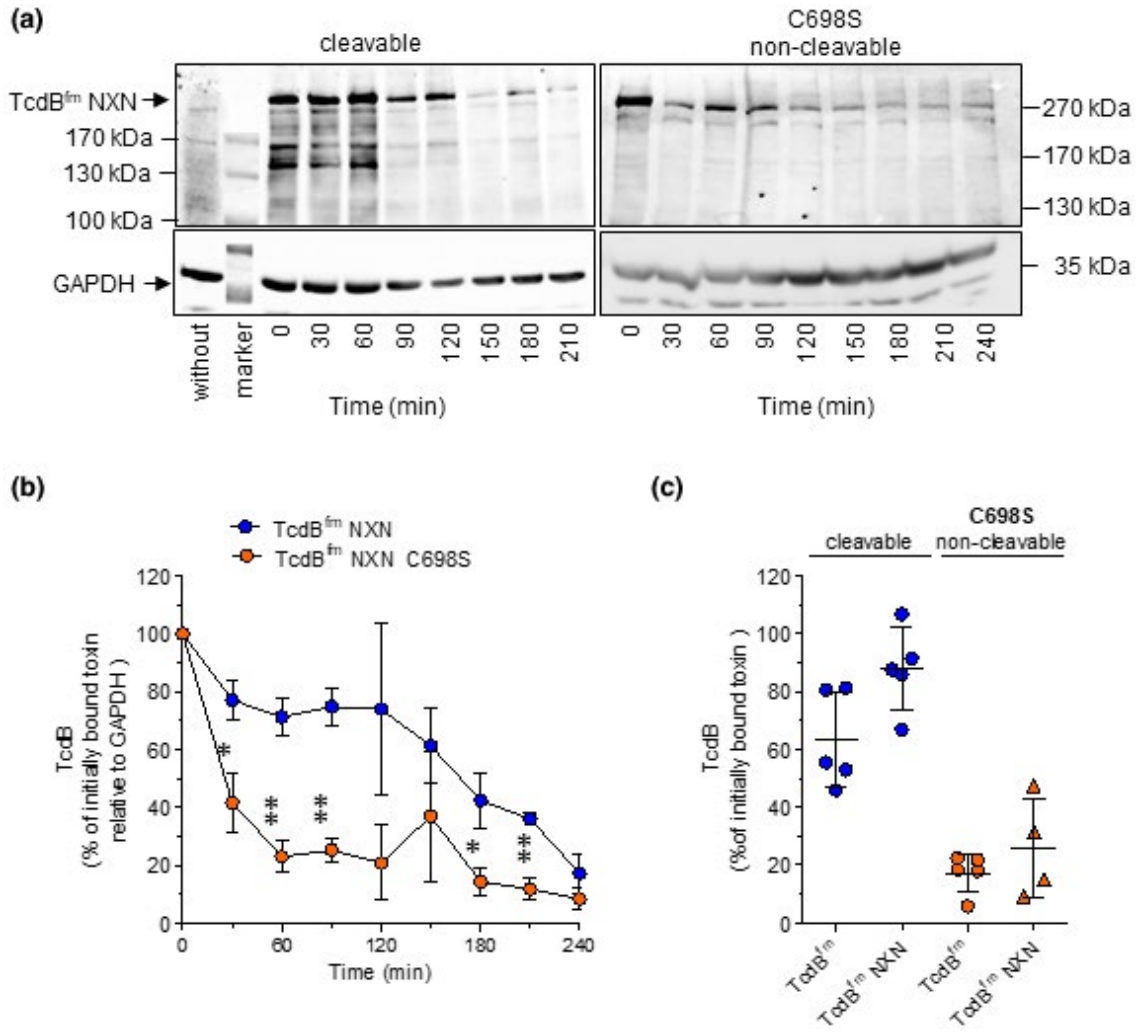

FIGURE 2 Degradation of full length TcdB. (a) Immunoblots of TcdB^{fm} NXN and the non-cleavable TcdB^{fm} NXN C698S in whole cell lysates of HEp-2 cells detected by polyclonal rabbit α-TcdB antibody. Shown is a representative time course over 4 hr. GAPDH was used as loading control. (b) Densitometrical evaluation of 3–8 independent experiments as shown in (a). (c) Comparison of cleavable and non-cleavable (C698S) TcdB^{fm} with and without (NXN) glucosyltransferase activity 30 min after starting pulse assay. Shown are means ± SE, $n = 5$

C698S, TcdB^{fm} NXN C698S). These experiments reveal that the clearance of TcdB in HEp-2 cells is diminished somehow, meaning it is less efficient as it ought to be.

2.3 | TcdB colocalizes with LAMP1

To verify our hypothesis of reduced lysosomal degradation of TcdB we validated the endo-lysosomal route for TcdB by colocalization with the marker protein lysosome-associated membrane glycoprotein-1 (LAMP1). Again, we used GT-deficient TcdB (TcdB NXN) to circumvent cell rounding induced by Rho glucosylation. Using confocal fluorescence microscopy, we found clear colocalization of TcdB with LAMP1 in a number of spots as early as 30 min after allowing TcdB uptake, and this was still evident after 60 min (Figure 3). In accordance with Figure 2 there was almost no TcdB^{fm} NXN C698S detectable within the cells after 120 min. In contrast, cleavable TcdB^{fm} NXN was detected in or at vesicular structures even after 120 min. It is unclear whether this was the remaining, non-degraded trunk of TcdB within the endo-lysosomes, or if it was the cleaved GTD associated to the vesicle membranes on the cytosolic site. This could not be resolved since we used our purified polyclonal anti-TcdB IgG which recognizes multiple epitopes within all functional domains of TcdB, including the GTD. Neither the flag-tag nor the myc-tag fused to the GTD was recognized by specific antibodies in immunofluorescence to a signal strength beyond background fluorescence and, thus, was proven to be insufficient for immunofluorescence microscopy under experimental set up.

2.4 | TcdB impairs lysosomal function

Having demonstrated that TcdB co-localizes with LAMP1 we then tested lysosomal function by using a DQ-BSA degradation assay to

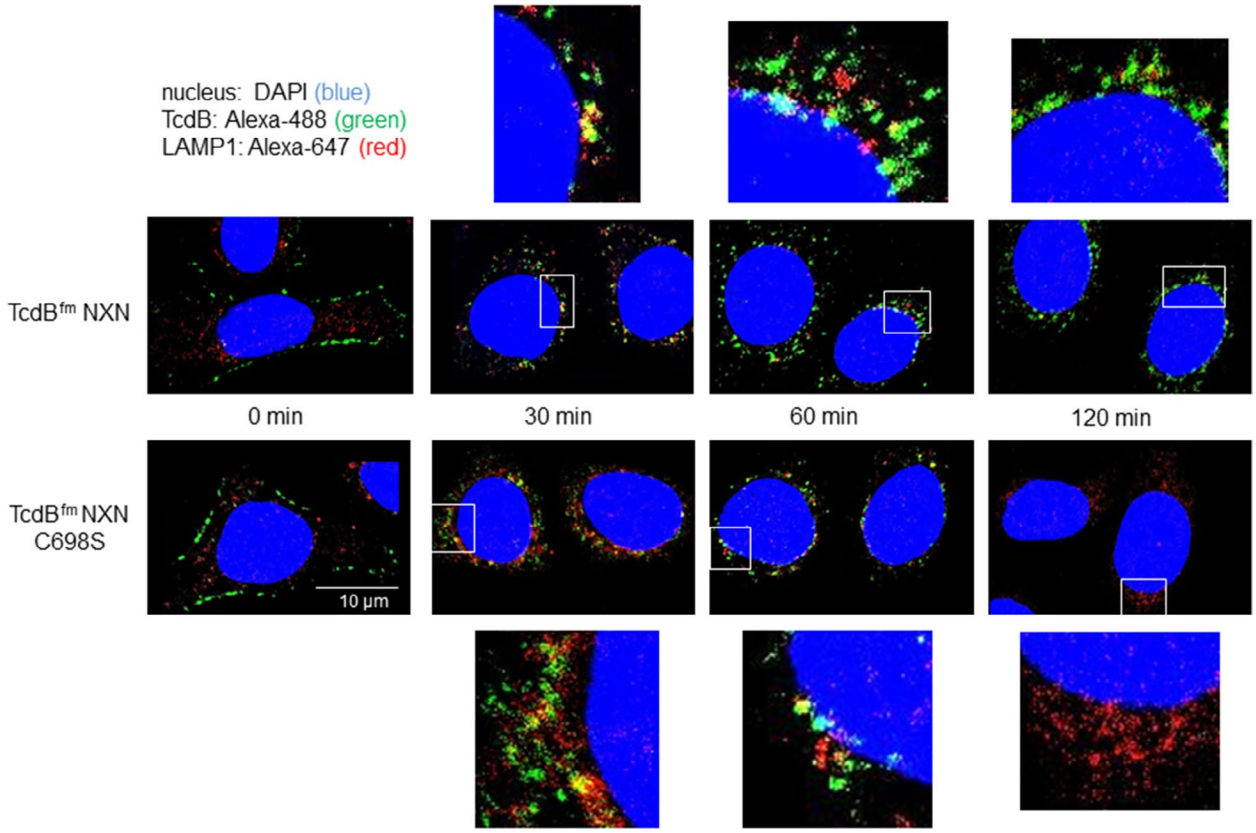

FIGURE 3 Colocalization of TcdB and LAMP1. Confocal laser scanning microscopy of TcdB (polyclonal rabbit anti-TcdB IgG; green) and the lysosome marker LAMP1 (anti-LAMP1; red) after binding (0 min) and after uptake for 30, 60, and 120 min. TcdB^{fm} NXN as well as TcdB^{fm} NXN C698S show colocalization with LAMP1 after 30 and 60 min. The marked areas are shown in higher magnification for better resolution

evaluate the proteolytic capacity of the lysosomal compartment. BSA labeled with a high concentration of BODIPY dye (DQ Green-BSA) self-quenches until it is degraded within the lysosomes. Degradation of the labelled BSA to peptides abolishes self-quenching, resulting in an increase of fluorescence, which directly correlates with lysosomal proteolytic activity. We used DQ-Green BSA for the endo-lysosomal route to follow degradation of cargo in HEp-2 as well as in DonQ cells. As depicted in Figure 4a, HEp-2 cells but not DonQ cells round up after treatment with TcdB. DonQ cells are a mutant CHO cell line devoid of UDP-Glucose, which is the essential co-substrate for TcdB-catalyzed Rho-glucosylation (Chaves-Olarte et al., 1996). The DonQ cells enabled us to perform confocal laser scanning microscopy in cells without changed cell morphology when treated with wildtype TcdB. As reported previously, DonQ cells do not round up when treated with TcdB, albeit the cells are as sensitive as HEp-2 cells regarding necrotic cell death, also termed pyknosis, when treated with high concentrations of TcdB (Beer et al., 2018a, 2018b). This phenomenon verifies toxin uptake into the cells, although no cell rounding or glucosylation of Rho-GTPases can be detected. Since we observed a delay in degradation of the GT-deficient TcdB mutant (TcdB NXN, see Figure 1) we initially test the impact of TcdB^{fm} NXN on degradation of DQ-BSA in HEp-2 cells. In DQ-BSA-treated cells there were plenty of vesicular structures with bright green fluorescence detectable after 4 hr incubation (Figure 4b). Notably, fluorescence was strongly reduced in cells treated with TcdB^{fm} NXN, indicating reduced degradation of endolysosomal DQ-BSA. The DQ-BSA fluorescence in HEp-2 cells treated with non-cleavable TcdB^{fm} NXN C698S was comparable to what was found in DQ-BSA loaded cells without toxin, indicating functional and fully active lysosomes in these cells. These findings are in line with degradation kinetics of TcdB NXN and TcdB NXN C698S shown in Figure 2. To ensure that our findings are not an artefact based on structural changes in TcdB due to mutated Mn^{2+}-binding site (D286/288N; NXN), we performed an additional DQ-BSA assay in DonQ cells. We found that GT-proficient toxin also induced lysosomal dysfunction in the DonQ cell line, demonstrating that this novel GT-independent feature of TcdB is not restricted to HEp-2 cells. It is assumed to be a general feature associated with endocytosis of TcdB.

We then used different mutant forms of TcdB to test known features of the toxin for their contribution to decreased lysosome degradation capacity. We initially tested the requirement for glucosyltransferase activity by assessing DQ-BSA degradation in HEp-2 cells and in DonQ treated with TcdB without or with glucosyltransferase activity, respectively (Figure 4c,d). We confirmed that the effect on lysosomes was not due to the 3 × flag/myc-tag, since TcdB NXN was as potent in inhibition as TcdB^{fm} NXN. Quantification of DQ-BSA fluorescence also revealed that the lysosome function in HEp-2 cells treated with non-cleavable TcdB^{fm} NXN C698S did

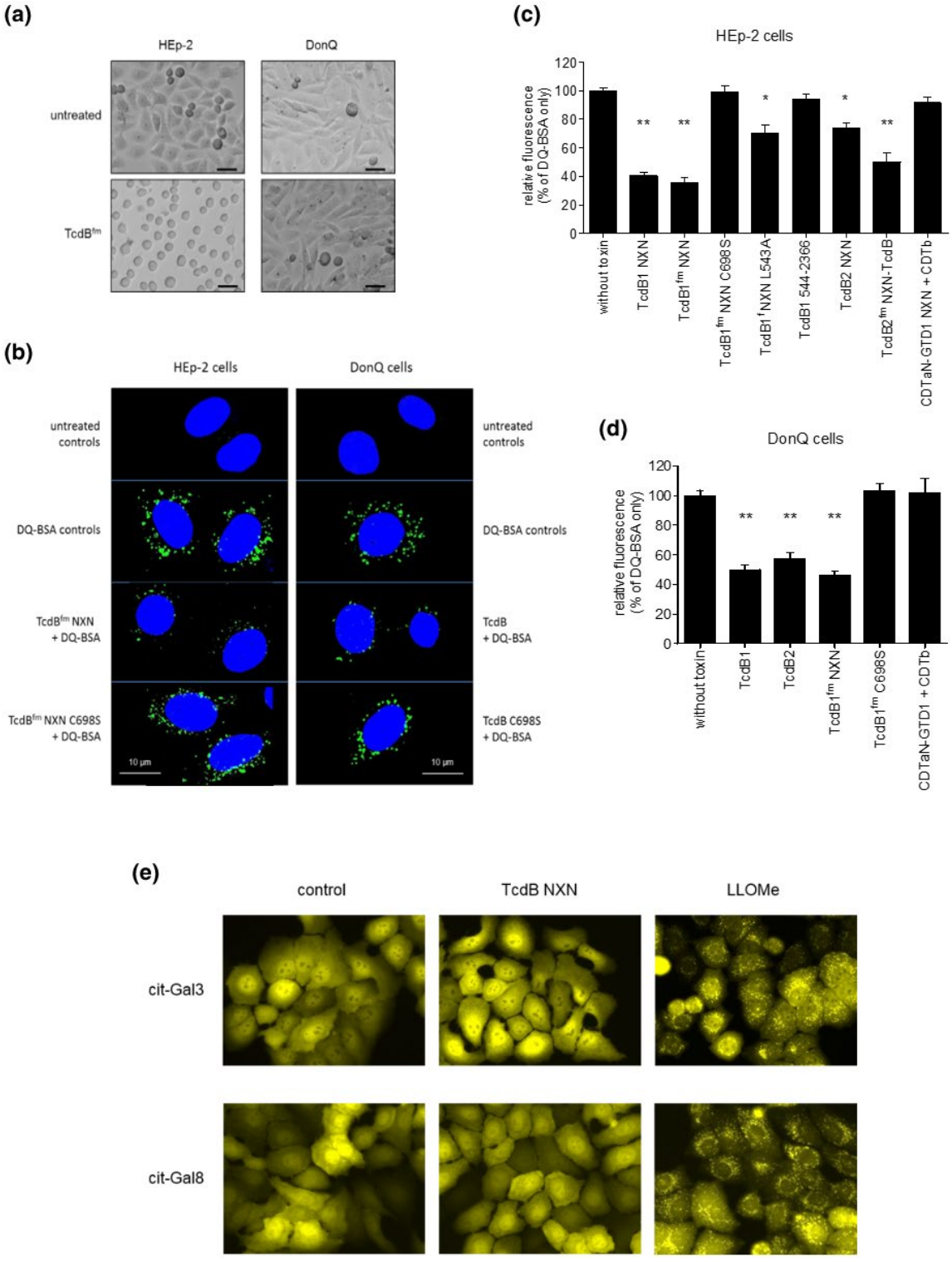

FIGURE 4 TcdB decreases lysosomal degradation capacity. (a) Micrographs show morphological changes of HEp-2 cells and DonQ cells, which are devoid of UDP-glucose, after treatment with $TcdB^{fm}$. Scale bar: 20 µm. (b) Confocal fluorescence microscopy of DQ-Green BSA assay in HEp-2 and DonQ cells (nuclei stained blue with DAPI). $TcdB^{fm}$ NXN but not $TcdB^{fm}$ NXN C698S reduced lysosomal degradation of DQ-Green BSA compared to controls. (c, d) Quantification of DQ-Green BSA fluorescence in HEp-2 and DonQ cells treated with indicated toxins for 4 hr. Shown are means ± SE, $n = 4–10$. (e) HEp-2 cells transfected with citrine-Galectin-3 (cit-Gal3) and citrine-Galectine-8 (cit-Gal8) were treated with 600 ng/ml TcdB NXN or with 10 mM LLOMe as positive control for lysosome membrane damage

not differ from untreated controls. By application of a second non-cleavable mutant ($TcdB^{F}$ NXN L543A) we confirmed release of the GTD as major requirement for interference with lysosomal function (Figure S2). TcdB with active CPD but without GTD (TcdB 544-2366, or TcdB ΔGTD) also had no effect on lysosomes in our study. We found that TcdB2 NXN diminished DQ-BSA degradation, but to a

lesser extent than TcdB NXN. This is possibly due to less efficient uptake, since TcdB2 does not interact with frizzled 1,2,7 and is only taken up into cells via CSPG4 (Chen et al., 2018; Chung et al., 2018; Henkel et al., 2020). The chimeric TcdB possessing the GTD of TcdB2 (TcdB2^{fm} NXN-TcdB) was even more potent than holo-TcdB2 NXN, emphasizing that the CPD-catalyzed release of the GTD but not the GTD itself is important for the effect on the lysosomes. This was cross checked by delivering the GTD of TcdB1 into HEp-2 cells by exploiting the binary CDT delivery system (Beer et al., 2018a, 2018b). A schematic of CDT delivery system is shown in Figure S3. CDTaN-GTD1 NXN + CDTb did not affect lysosomal degradation of DQ-BSA. Intracellular delivery of the GTD was checked in parallel by a cell rounding assay using CDTaN-GTD1 + CDTb (Figure S3). DonQ cells verified that the observations made for GT-deficient mutant of TcdB were also true for active toxins: TcdB1 and TcdB2 were as potent as TcdB^{fm} NXN, which was used as positive control. Neither non-cleavable TcdB (TcdB^{fm} C698S) nor the isolated intracellular GTD1 (CDTaN-GTD1 + CDTb) had an effect on degradation of DQ-BSA since fluorescence was unchanged compared to untreated controls. Beside this, CDTb which oligomerizes and forms a pore for translocation of CDTa, was obviously unable to affect lysosome function, verifying a specific effect for TcdB and putatively other homologous glucosyltransferases. Thus, only TcdB which can release the GTD but not the released GTD itself affects lysosomes. Table 1 summarizes mutant toxins and their respective features associated with reduced lysosomal degradation capacity.

Despite lack of negative effect of CDTb on lysosomes it cannot be excluded that membrane insertion and pore formation by TcdB disrupts endolysosomal membrane integrity, thereby leading to loss of function of the lysosomes. To test this, we transfected HEp-2 cells with citrine labeled galectin-3 and galectin-8 (cit-Gal3, cit-Gal8). Galectin-3 and -8 bind to lysosomes when luminal carbohydrate structures are exposed to the cytosol in case of lysosomal membrane damage (Hasegawa et al., 2015; Jia et al., 2020). Figure 4e shows cit-Gal3 and cit-Gal8 transfected HEp-2 cells treated with TcdB NXN. Both galectins are diffusely distributed within the cytosol and nucleus of untreated cells. Application of TcdB (600 ng/ml) for up to 5 hr did not induce translocation or accumulation of cit-Gal3 or cit-Gal8 to lysosomal compartments, indicating full membrane integrity of lysosomes. Only few puncta could be detected in some cells. The number of these puncta was however in the same range as in untreated control cells of approximately 1 per 10 cells. Accumulation of cit-Gal3 and cit-Gal8 at endolysosomal compartments within the perinuclear region was however clearly visible after incubation of cells with 10 mM LLOMe, which served as positive control for lysosomal damage, even after 2 hr incubation. These findings support a hypothesis of specific manipulation of lysosomes by TcdB rather than mere disruption of their membrane integrity.

2.5 | Inhibition of lysosomal function is associated with altered detection of LAMP1

In the time course of toxin uptake (see Figure 3) a weaker detection of LAMP1 might be postulated in cells that were treated with cleavable toxin (TcdB^{fm} NXN) compared to non-cleavable TcdB (TcdB^{fm} NXN C698S). Single channel pictures of confocal microscopy in Figure S4 show pictures with amplified intensity. It was unclear whether abundance of LAMP1 has changed or if distribution of LAMP1 was altered by TcdB. We therefore switched from confocal fluorescence microscopy to standard fluorescence microscopy for a more comprehensive analysis. Whereas the overall signal in immunofluorescence was not decreased, a clear translocation of LAMP1 positive structures was observed in response to toxin treatment. Quantification of the fluorescence signal along sagittal section planes of HEp-2 cells revealed accumulation of LAMP1 in the perinuclear region when cells were treated with TcdB NXN (Figure 5a). Translocation of LAMP1 resulted in significantly different profiles of fluorescence signals, whereas fluorescence of the core nuclear region was not altered (Figure 5b). By using Lysotracker™ Green we also quantified functional lysosomal structures in toxin treated HEp-2 cells. After incubation of cells with TcdB NXN alone for 2 hr and additional 2 hr in the presence of Lysotracker™ Green there was a significant decrease in fluorescence, indicating reduced number of functional lysosomes compared to untreated cells. This finding was even more evident after 3 hr toxin treatment plus further 2.5 hr incubation with Lysotracker™ Green. Representative micrographs are shown in Figure 5c and quantification of fluorescence under both conditions are shown in Figure 5d. Since results from Lysotracker™

TABLE 1 Summary of toxin features associated with lysosome inhibition

	Feature				
Toxin	GTD active	CPD active	Cytosolic GTD	Cell rounding	Lysosome inhibition
TcdB	✓	✓	✓	✓	✓
TcdB NXN		✓	✓		✓
TcdB C698S	✓		✓	✓	
TcdB NXN C698S			✓		
TcdB NXN L543A		✓	✓		✓
TcdB 544-2366		✓			
CDTaN-GTD + CDTb	✓		✓	✓	

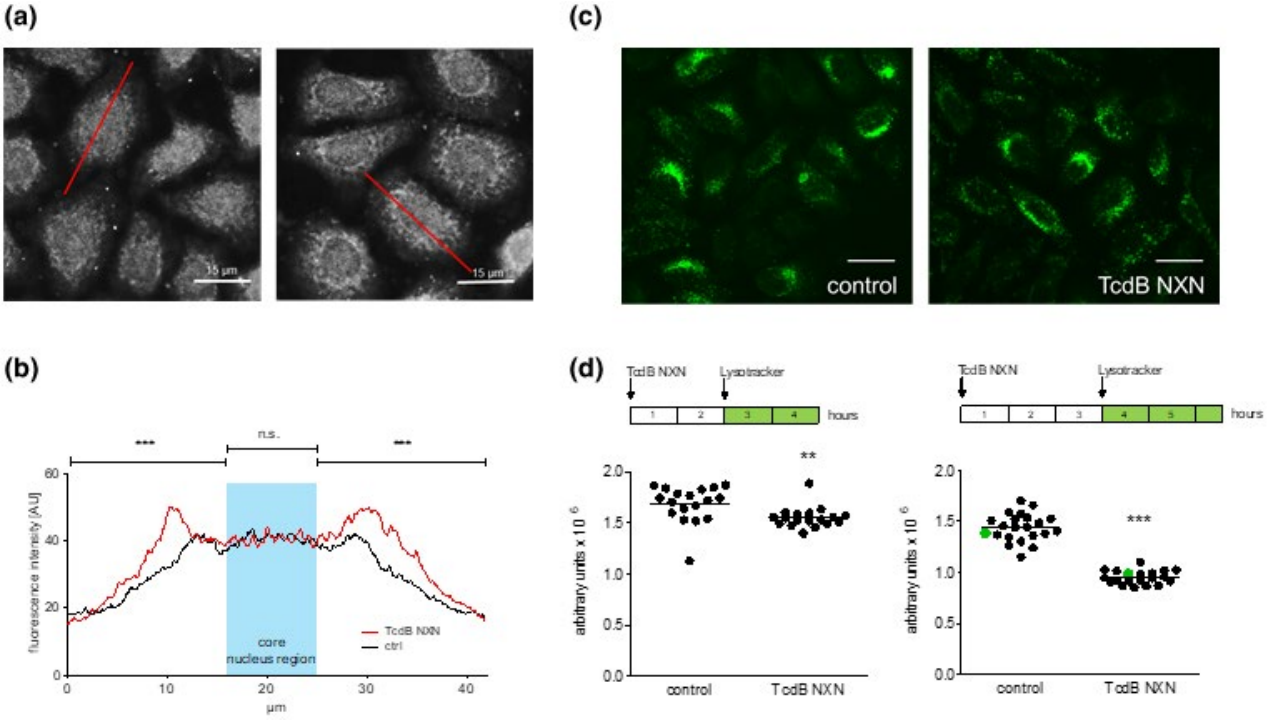

FIGURE 5 Detection of lysosomes by LAMP1 staining and LysoTracker. (a) Fluorescence staining of LAMP1 was performed to identify lysosomal structures. Red line indicates sagittal section plane to quantify fluorescence profile as shown in (b) (scale bar = 15 µm). (b) Mean profiles of fluorescence from single cells of untreated controls and HEp-2 cells treated with 600 ng/ml TcdB NXN for 6 hr ($n = 36$; *** $p < .0001$; n.s. = non-significant). (c) Lysosome staining by LysoTracker Green DND-26 after treatment of HEp-2 cells with TcdB. Scale bar in representative micrographs represents 25 µm. Cells were incubated with or without TcdB NXN (600 ng/ml) for 3 hr and further 2.5 hr in the presence of LysoTracker. (d) Quantification of fluorescence signal after 4 hr incubation with TcdB ($n = 18$). Quantification of fluorescence signal after 5.5 hr incubation with TcdB ($n = 18$). Green data points C correspond to representative micrographs shown in (c)

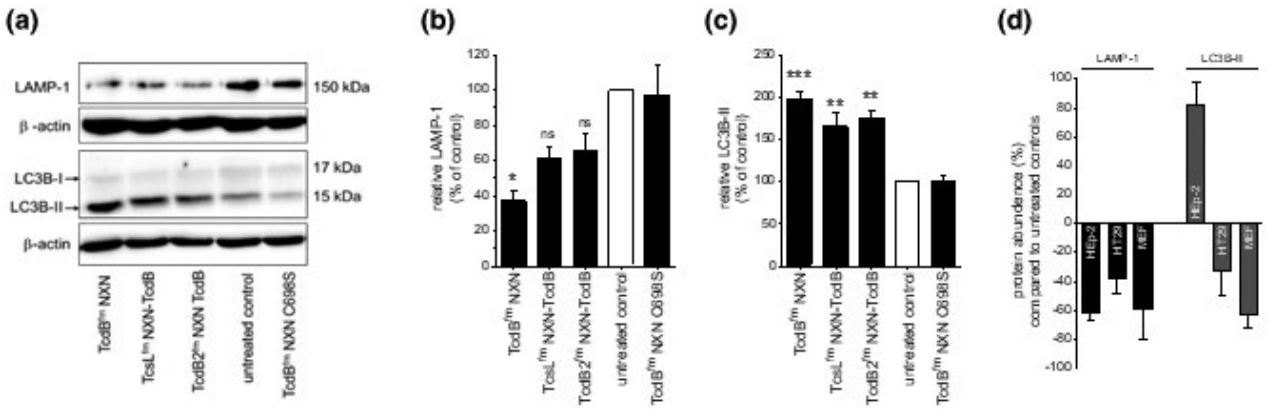

FIGURE 6 Decreased lysosome function is associated with changes in LAMP1 and LC3B-II. (a) Representative immunoblots show lysosomal marker protein LAMP1 of 150 kDa detected by polyclonal anti-LAMP1 and the autophagosome marker protein LC3B-I and LC3B-II in HEp-2 cells after treatment with $TcdB^{fm}$ NXN as well as the chimeras $TcsL^{fm}$ NXN, $TcdB2^{fm}$ NXN and the non-cleavable mutant $TcdB^{fm}$ NXN C698S. (b, c) The corresponding densitometrical evaluation of LAMP1 from three independent experiments as shown in (a). Indicated significances refer to $TcdB^{fm}$ NXN C698S. Right graph shows evaluation of only LC3B-II. Shown are means ± SE, $n = 4–15$. (d) LAMP1 and LC3B-II were also measured by immunoblot in HT29 cells and mouse embryonic fibroblasts after treatment with 600 ng/ml TcdB NXN. LC3B-II increased only in HEp-2 cells but was decreased in HT29 and MEF. Shown are means ± SE, $n = 5–15$

Green do not correlate with LAMP1 immunofluorescence staining, we additionally checked LAMP1 level in western blot analyses. Figure 6 shows detection of LAMP1 in whole cell lysates of HEp-2 cells treated with different toxin mutants. Immunoblot analyses were performed with polyclonal anti-LAMP1 recognizing a heavily glucosylated 150 kDa sized form of this protein. In addition, we also performed immunoblots with monoclonal anti-LAMP1 (clone E-5) recognizing two approximately 130 kDa sized

glucosylated forms of LAMP1 (Figure S5). Both antibodies showed weaker signals for LAMP1 in cells treated with glucosyltransferase deficient TcdB ($TcdB^{f}$ NXN). The discrepancy between detection of LAMP1 in immunofluorescence staining and in immunoblots cannot be explained without further research and knowledge about LAMP1 function. We hypothesize that the effect of TcdB on the lysosomes affects solubility of LAMP1 leading to a weaker detection in Western blot analyses. Therefore, LAMP1 still was taken as surrogate for effect of TcdB on lysosomes to screen further toxins for their interference with lysosome function. Weaker detection of LAMP1 was also observed in cells treated with the chimeras $TcdB2^{fm}$ NXN-TcdB and $TcsL^{fm}$ NXN-TcdB, although to a lesser extent (Figure 6a,b). The glucosyltransferase domain of TcsL from *Paeniclostridium sordellii* strain 6018 showed high homology to TcdB (74.8% identity). Due to high standard deviation in this set of experiments, the effects of both chimeras on lysosomes were not significant. Again, non-cleavable TcdB ($TcdB^{fm}$ NXN C698S) had no effect on lysosomal marker of HEp-2 cells. To exclude that the cysteine protease activity affects lysosomes by cleavage of a yet unknown endogenous substrate, we also tested $TcdB^{f}$ NXN L543A, which is a different non-cleavable mutant with full cysteine protease activity. $TcdB^{f}$ NXN L543A was significantly less potent regarding inhibition of lysosomes than $TcdB^{fm}$ NXN but not completely inactive (Figure S6).

Not only endocytotic cargo but also other intracellular proteins as well as organelles are metabolized or recycled by lysosomes. Decreased lysosomal function thus might also affect autophagosomes in consequence. We therefore tested TcdB and the negative control TcdB C698S, again, in order to correlate the change in LAMP1 detection with the autophagosome marker protein LC3B. The reduction of LAMP1 in $TcdB2^{fm}$ NXN-treated cells positively correlated with an increase in LC3B-II (Figure 6c). Again, the chimeras $TcdB2^{fm}$ NXN-TcdB and $TcsL^{fm}$ NXN-TcdB had a similar effect compared to $TcdB^{fm}$, although they were not as potent.

By testing various cell lines, we found that TcdB reduced LAMP1 in all cell lines tested so far. Representatively shown in Figure 6d are the human intestinal crypt cell line HT29 as well as mouse embryonic fibroblasts (MEF). As in HEP-2 cells, TcdB significantly reduced LAMP1 in the human intestinal epithelial crypt cell line HT29 cells and also in MEF. Although TcdB increased LC3B-II in HEp-2 cells, LC3B-II was reduced in TcdB-treated HT29 cells and MEFs to a comparable extent as LAMP1.

2.6 | The TcdB effect on lysosomes is independent of necrotic calcium signaling

At this point we have established that release of the GTD but not the released GTD itself is a prerequisite for reduction in lysosomal degradation capacity. We assumed that the release of the GTD from the trunk of TcdB unblocks a pore built by TcdB through which the GTD has passed. Interestingly, very recently a screen for small compound inhibitors revealed calcium channel signaling as mediator for a glucosyltransferase-independent necrotic effect of TcdB (Farrow et al., 2013, 2020). In that screen calcium channel inhibitors of the dihydropyridine type were identified as protective compound against TcdB-induced necrosis. We therefore tested the therapeutically used dihydropyridine derivative nifedipine as classical L-type calcium channel blocker. In accordance with literature, 10 μM nifedipine completely abolished the necrotic effects of TcdB in our study, i.e. chromatin condensation and blistering, and inhibited early cell death as additionally shown by DAPI incorporation (Figure 7a,b) (Wohlan et al., 2014). To our surprise, nifedipine did not abolish TcdB effect on lysosomes as it did not prevent the decrease in LAMP1 (Figure 7c) and, accordingly the increase in LC3B-II (Figure S7). In line with this, nifedipine also did not affect detection of TcdB (Figure 7d,e). We conclude that calcium signaling by L-type calcium channels, which may trigger TcdB-induced early cell death, is not the reason for reduced lysosomal function, albeit the underlying mechanism to trigger both phenomena might be the same. This was also evident by testing TcdB with different receptor specificities. Sufficient uptake of TcdB to affect lysosomes was only achieved via CSPG4, as it was shown for induction of pyknosis before (Figure S8) (Henkel et al., 2020).

3 | DISCUSSION

The present study describes the inhibition of lysosomal activity as a novel feature of *C. difficile* TcdB. The effect on lysosomes is independent of the glucosyltransferase activity and, thus, independent of Rho GTPase glucosylation. The decreased lysosomal degradation capacity was determined by the DQ-Green BSA assay and correlated with decreased staining of functional lysosomes with LysoTracker™-Green. The diminished lysosome activity was also associated with accumulation of LAMP1 to the perinuclear region of cells and with altered detection of LAMP1 in Western blot analyses. The discrepancy between immunofluorescence staining and Western blot analyses of LAMP1 reflects the important question whether TcdB decreases lysosomal structures (number of lysosomes) or function (lysosomal capacity) in this fluid system of intracellular vesicles. We assume that decreased solubility of LAMP1 in TcdB treated cells or other secondary effects reduce recognition of LAMP1 by specific antibodies in Western blot analyses. Our immunofluorescence data do not support findings from Western blots. However, immunofluorescence showed clear translocation of LAMP1 to the perinuclear region in toxin-treated cells. The translocation is comparable to the galectin-3, -8 staining of damaged lysosomes that were affected by LLOMe. To substantiate our hypothesis that a decrease in LAMP1 is not the cause for TcdB-induced lysosomal dysfunction we analyzed proteome data from a former study where the (phospho) proteome of HEp-2 cells treated with TcdB and TcdB NXN was investigated (Junemann et al., 2018). The supplementary table 1 to that study lists LAMP1 as not significantly affected in abundancy after treatment of

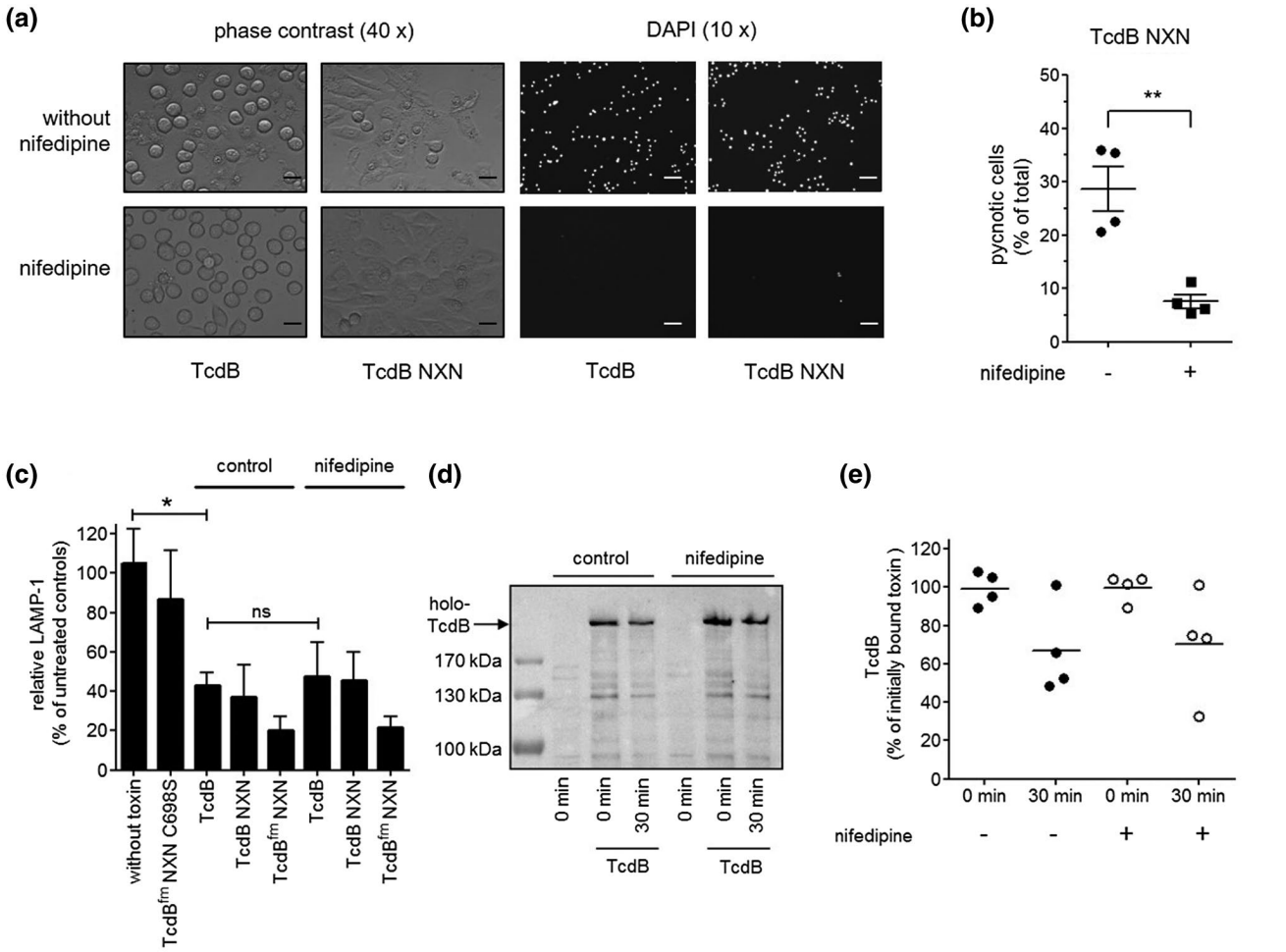

FIGURE 7 Nifedipine abolishes necrotic cell signaling but not lysosomal dysfunction. (a) Hep-2 cells show about 40% DAPI positive cells after treatment with 600 ng/ml TcdB or TcdB NXN in a pulse assay, which was completely abolished by 10 μM nifedipine. Phase contrast micrographs are shown left (scale bar: 25 μm) and fluorescence pictures of incorporated DAPI into dead cells are shown right (scale bar: 100 μm). (b) Quantification of 4 independent experiments as shown in (a). (c) Densitometrical evaluation of LAMP1 immunoblots from 4–8 independent experiments. Shown are means ± SE. Nifedipine did not significantly affect reduction of lysosomal marker protein LAMP1 by TcdB. (d) Immunoblot showing degradation of TcdB after 30 min in the presence or absence of nifedipine. (e) Densitometrical evaluation of 4 independent experiments as shown in (d)

HEp-2 cells with TcdB or TcdB NXN for 8 hr with comparable concentration as used here in this study.

The effect of TcdB on lysosomal function correlated with changes in the autophagosome marker LC3B-II as surrogate for altered autophagic flux in HEp-2 cells. It is unclear whether TcdB directly affects autophagic flux, or if it is secondary to lysosomal dysfunction. We found that in HT29 cells and MEF TcdB decreased detection of LAMP1 and also affected LC3B-II, validating effect of TcdB on lysosomes and on the autophagic flux in various cell lines. It seems, however, that the effect on autophagic flux depends on specific conditions and the respective cell line, since we observed an increase as well as a decrease in LC3B-II, depending on cell line. Further studies are required to correlate altered LC3B-II level with disturbance in autophagic flux and the functional outcome of the altered abundance of this surrogate marker.

The precise mechanism of this novel effect of TcdB is not clear, yet. We aimed at characterizing the preconditions leading to inhibition of lysosomes by applying different mutant and chimeric forms of TcdB. Obviously, the effect appears independently of Rho-GTPases and Rho glucosylation, as wildtype TcdB as well as glucosyltransferase-deficient TcdB inhibited lysosome function to the same extent. Since TcdB lacking the GTD had no effect, we postulate insertion of the N-terminal region of TcdB into the endosomal membrane as a prerequisite. This assumption is supported by the different chimeric TcdB variants harboring either the GTD of TcdB from endemic strain R20291 or of TcsL from *P. sordellii* strain 6018, indicating that the GTD itself is not decisive. Beside insertion into the endosomal membrane a second feature mainly contributes: the autoproteolytic release of the GTD. If the GTD is not released by the cysteine protease domain, the effect on lysosomes is completely abolished. A second mutant (TcdB L543A) possessing an active cysteine protease but lacking a functional cleavage site showed significantly weaker effect on lysosomes. We discarded the hypothesis that the TcdB effect is due to cleavage of

an unknown intracellular host cell protein since TcdB lacking the CROPs also had no effect on lysosomes. Furthermore, the chimeric TcdB2^{fm}-TcdB and TcsL^{fm}-TcdB possess the identical cysteine protease domain as TcdB^{fm}, but none the less differentially inhibited the lysosomes. Based on our findings we prefer the hypothesis of a pore built by pH-dependent membrane insertion of TcdB as described for TcdA (Giesemann et al., 2006; Orrell et al., 2017, 2020). This transient pore might last when unblocked by release of the GTD, which is not the case in artificial lipid bilayer assays. The orientation of the GTD in respect to the rest of the toxin which spans the endosomal membrane seems to be crucial for triggering lysosomal dysfunction. Whatever affects cytosolic translocation and autoproteolytic release of the GTD also affects interference of TcdB with lysosome function. In summary, the amount of TcdB, the translocation kinetic and the release of the GTD are the major parameters that are decisive for reduced lysosomal capacity. It needs to be clarified whether the decrease in LAMP1 results from a decay of lysosomes, reduced lysosome recycling or from abrogated vesicle fusion processes or a decrease in lysosomal biogenesis. First data obtained with LysoTracker™-Green speak for a decrease in number of functional lysosomes.

The observed effect on lysosomes is linked to endosomal egress of TcdB. We hypothesize an underlying mechanism that also accounts for the early necrotic cell death. Early cell death is only triggered when sufficient TcdB rapidly enters cells, before sufficient Rac1 is glucosylated (Beer et al., 2018a, 2018b). As shown, inhibition of Rac1 prevents TcdB-induced necrotic signaling. A rapid flush of TcdB can only be achieved by a high uptake rate, which is mainly accomplished by CSPG4 in our HeLa and HEp-2 cell culture model (Henkel et al., 2020). Uptake via CSPG4 alone is sufficient to affect lysosomes as shown by mutant TcdB F1597S and endemic TcdB2 (R20291), which both do not interact with frizzled 1,2,7 (Chen et al., 2018; Chung et al., 2018; Henkel et al., 2020). Uptake into cells solely by frizzled 1,2,7 does not provoke this effect in HEp-2 cells as shown in Figure S8 by using TcdB1-1832, which does not interact with CSPG4 (Henkel et al., 2020; Tao et al., 2016). Beside receptors, facilitation of acidification of the endosomal lumen by sodium and chloride flux also supports toxin translocation, thereby enhancing cytopathic and cytotoxic effects especially of TcdB (Beer et al., 2018a, 2018b; Ruhe et al., 2017). The early cell death can only be executed in the presence of signaling competent Rac1 and NADPH oxidase and is triggered by necrotic calcium signaling (Beer et al., 2018a, 2018b; Farrow et al., 2013, 2020). Yet, we do not know whether the underlying mechanism for early cell death and the novel observed impairment of lysosomal function is identical. The latter does not involve L-type calcium channels and thus cannot be inhibited by specific blocker. Further studies have to be performed to define the mechanism and to show involvement of calcium signaling independent of L-type channels. Preincubation of cells with nifedipine enabled us to dissect between pyknotic/necrotic effects and lysosome inhibition accompanied with proposed secondary accumulation of autophagosomes. It has to be emphasized that impairment of lysosomes by TcdB can be observed in cells that do not suffer early necrotic cell death, meaning a new quality in TcdB-induced cell damage.

One possible interpretation of the observed increase in LC3B-II in TcdB-treated cells can be an accumulation of autophagosomes. This is to be expected when lysosomal degradation processes are impaired and the autophagic flux is interrupted. On the other hand, increased synthesis of LC3B can also be taken as marker for increased autophagosome formation required for autophagy of dysfunctional lysosomes. To date, two reports describe TcdB-triggered autophagy (Chan et al., 2018; He et al., 2017). Both studies showed that changes autophagy and in autophagic marker were associated with the glucosyltransferase activity of TcdB. However, the interpretation of LC3B signals in immunoblots is critical without additional autophagic assays (Barth et al., 2001, 2010; Mizushima & Yoshimori, 2007). This was evident in our study when cells of different origin were used. Whereas the effect on LAMP1 was the same in all tested cell lines, the effect on LC3B-II varied among different cell lines. The overall impact of TcdB on autophagosome formation and degradation has to be investigated in follow up studies. At the moment it is unclear how impairment of lysosomal function contributes to pathogenicity of *C. difficile* infections. According to recent findings published by Bilverstone and coworkers the glucosyltransferase activity of TcdB is required for pathogenesis (Bilverstone et al., 2020). Thus, the necrotic effect and impairment of lysosomes are not the priority mechanisms leading to clinical symptoms. It can however be assumed that glucosyltransferase-independent effects modulate pathogenic effects or come into play only in a subset of target cells. Like what is known for pyknotic effect, a high uptake rate is also required for immediate block in lysosomal function, since only CSPG4-mediated uptake but not uptake via frizzled 1,2,7 alone warranted this effect in HEp-2 cells. It can be assumed that preferentially phagocytic cells with high endocytotic activity will be affected by this novel feature of TcdB.

4 | EXPERIMENTAL PROCEDURE

4.1 | Cloning and heterologous expression of large clostridial glucosyltransferases

All large clostridial glucosyltransferases have been produced using the *Bacillus megaterium* expression system (MoBiTec) as was described for TcdA, TcdB, and TcsL (Burger et al., 2003; Tian et al., 2020; Wohlan et al., 2014). All genes were sequenced an coded for proteins or fragments of proteins according to following accession numbers: TcdB *C. difficile*_VPI10463: WP_009895693.1; TcdB *C. difficile*_R20291: CBE02479; TcsL *P. sordellii*_6018: Q46342.1; Cloning of the glucosyltransferase-deficient TcdB was done by site directed mutagenesis as was also described by Wohlan and coworkers (Wohlan et al., 2014). Chimeras of TcdB with various flag/myc-tagged glucosyltransferase domains were generated by introducing a BamHI restriction site in TcdB at position 1621–1626. This silent mutation enables us to exchange the coding sequence for the GTD

without alteration of the amino acid sequence Gly-Ser directly upstream of the autoproteolytic cleavage site. By opening the BamHI restriction site and filing in oligonucleotides coding for a combined 3 × flag- and a myc-tag with compatible overhangs for 5′ BamHI and 3′ BglII we obtained a single BamHI restriction site directly 5′ of the flag tag to insert various GTDs. All GTDs used for building chimeras were amplified by PCR with 5′ restriction site for BsrGI and 3′ site for BamHI and ligated into the expression vector pHIS1522_TcdB, modified as described above via BsrGI/BamHI. Generation of TcdB C698S and TcdB L543A was done by site directed mutagenesis kit from Staratgene, using following sense and antisense primer: TcdB C698S_sense: 5′-GAAATAAATTTATTAGGATCTAATATGTTTAGCT ACTCTATCAACG-3′, TcdB C698S_anti: 5′-CGTTGATAGAGTAGCTA AACATATTAGATCCTAATAAATTTATTTC-3′, TcdB L543A_sense: 5′ -CAAGGATGACCATGACGGATCCGCTGGTGAAGATGATAATCTTG -3′, TcdB L543A_anti: 5′-CAAGATTATCATCTTCACCAGCGGATCCG TCATGGTCATCCTTG -3′.

Expression of all toxins and chimeras was done in 1 liter cultures of *B. megaterium* induced with 0.5% (w/v) xylose at an OD_{600} of 0.3. Cultures were agitated at 37°C for 4–5 hr and bacteria were pelleted by centrifugation, lysed by sonification and centrifuged again at 16,000 × *g*. The supernatant was sterile filtered (0.4 μm pore size), and toxins were purified by Ni^{2+}-affinity chromatography (Ni-IDA, Macherey-Nagel, Germany). Eluates containing highest toxin yield were passed through Zeba desalting columns (Pierce, ThermoScientific, Germany) for buffer exchange (20 mM Tris-HCl, pH 7.2, 50 mM NaCl). Concentration and purity of toxins was estimated by SDS-PAGE.

4.2 | Recombinant expression of CDT-fusion toxin

The binary toxin CDT from *C. difficile* strain R20291 was used to deliver the GTD from TcdB1 into cells. Therefore, the sequence of the N-terminal adapter domain of CDTa was fused in 5′-direction to the coding sequence of GTD1 (glucosyltransferase domain from TcdB1) in a pGEX2T-vector and expressed and purified as GST-fusion under standard condition as previously described (Beer et al., 2018a, 2018b). CDTaN-GTD1 was cleaved from immobilized GST by thrombin over night at room temperature. CDTb was cloned into pQE30 vector and expressed as N-terminal His-tagged protein. Purification was done by Ni^{2+}-affinity chromatography using Ni-IDA columns (Macherey-Nagel) and subsequent activation of purified CDTb was done by limited digestion with trypsin (0.2 μg trypsin/μg CDTb for 20 min at room temperature) as also described by Beer et al. (2018a, 2018b).

4.3 | Cell culture HEp-2 cells

In this study the human laryngeal epithelial cell line HEp-2 was used for the majority of experiments. Cells were kept in Minimal Essential Medium supplemented with 10% fetal bovine serum, 100 μM penicillin, and 100 μg/ml streptomycin. Cultures were split twice a week. In some experiments toxins with glucosyltransferase activity have to be tested in confocal microscopy. For these experiments the UDP-glucose deficient DonQ cells were used, since treatment with active TcdB does not result in Rho glucosylation and subsequent cell rounding (Chaves-Olarte et al., 1996). Chinese hamster ovary (CHO) DonQ cells were grown in Minimal Essential Medium with Earle's salts supplemented with 5 mM L-glutamine, 10% fetal bovine serum, 100 μM penicillin, and 100 μg/ml streptomycin.

4.4 | Retroviral transduction of HEp-2 cells

To produce the virus-containing supernatant 0.4 × 10^6 HEK293T cells were plated in 2 ml complete DMEM in one well of a 6 well dish. After 16–24 hr, HEK293T cells were transfected with retroviral constructs encoding a fusion protein of galectin-3 or galectin-8 with mCitrine (2 μg per well), the retroviral packaging plasmids gag-pol (1 μg well) and VSV-G (100 ng/well) using GeneJuice transfection reagent (Novagen, 70967). Cells were incubated at 37°C, 5% CO_2 for approximately 12 hr. Then the media was exchanged with DMEM containing 30% HI-FCS and cells were incubated for another 34 hr. After 36 hr, the viral supernatant was collected using a 10 ml Luer-lock syringe attached to a blunt 18G needle and then filtered using a 0.45 mm filter unit into a 50 ml falcon. The medium on Hep-2 cells was removed, and viral supernatant was added to the cells at a 2:1 ratio with complete DMEM. The cells were then incubated for approximately 24 hr at 37°C, 5% CO_2. The virus-containing medium was removed and replaced with complete DMEM. Transduced cells were passaged three times before frozen stocks were prepared.

4.5 | Treatment of cells in pulse assay

All experiments were performed as pulse assays. The appropriate toxin was added at given concentrations to the pre-cold cells at 4°C. Toxin was bound for 30 min at 4°C and non-bound toxin was removed by three wash steps with ice cold PBS. At time point 0 cells were moved to a 37°C chamber and incubated for 4 hr if not indicated otherwise.

For DQ-BSA assays, cells seeded on cover slips were washed with PBS and kept in culture medium without fetal bovine serum for 1 hr. Then, cells were preloaded with 10 μg/ml DQ-BSA for 1 hr before addition of toxins.

4.6 | Quantification of lysosomes by LysoTracker™ Green DND-26

HEp-2 cells were seeded onto coverslips at a density of $3{\cdot}10^4/cm^{-2}$. The next day, cells were treated with 600 ng/ml TcdB NXN. After 2 hr (or 3 hr) incubation, LysoTracker™ Green DND-26 was added at a final concentration of 500 μM for further 2 hr (2.5 hr respectively).

Then, cells were rinsed twice with PBS (37°C) and directly subjected to live cell microscopy to quantify fluorescence intensity of micrographs at 40× magnification. Therefore, an image with clear visible fluorescence was randomly chosen and a picture was taken using Leica software (Zen 3.1 blue edition) with automatic exposure time. All following micrographs of the experiment were taken under identical exposure time, ensuring complete data acquisition in less than 5 s to avoid bleaching of the region of interest. Each experiment was done in triplicate, choosing six different images of each repetition. The pictures were converted to JPEG files and ImageJ (version 1.53e) was chosen for quantification of mean fluorescence of each micrograph.

4.7 | Immunofluorescence staining and confocal laser scanning microscopy

Cells seeded on cover slips were washed with PBS and subsequently fixed in 4% paraformaldehyde in PBS at room temperature for 15 min (DQ-BSA assays) or in methanol for 15 min at −20°C (colocalization assay). Cells were washed three times with PBS. LAMP1 was directly stained by Alexa 647-conjugated monoclonal anti-LAMP1 antibody (1D4B, Santa Cruz) and TcdB indirectly via affinity-purified polyclonal anti-TcdB IgG (in house made [Henkel et al., 2020]) and Alexa 488-conjugated secondary antibody for 1 hr at room temperature, respectively. Cells were washed again and incubated with 150 μM DAPI (Serva) for nuclei staining at room temperature for 30 min.

Cells were embedded in mounting medium (Antifade Kit, Invitrogen) and analyzed by confocal laser scanning microscopy using an Olympus FluoView 1000 microscope (Research Core Unit for Laser Microscopy, MHH). For image acquisition, an Olympus FluoView 1000 confocal laser scanning microscope (Research Core Unit for Laser Microscopy, MHH) using a 60× oil immersion objective was used. Fluorescent dyes were excited at a wavelength of 491 nm (green fluorescence), 655 nm (red fluorescence) and 405 nm (blue fluorescence), respectively.

LAMP1 staining was also documented and analyzed by Zeiss microscopeAxio Observer 3/5/7 KMAT and software Zen version 3.1. Profiles of cells from 2 biological replicates from 3 independent experiments (36 cells in total) were analyzed.

4.8 | Western blot analyses

Cell lysates in Laemmli buffer were subjected to 7.5%–15% SDS-PAGE depending on size of protein of interest. Resolved proteins were transferred from gel onto nitrocellulose by semi-dry blotting at constant 17 V for 90 min. The nitrocellulose was rinsed with Ponceau solution (0.15% Ponceau S, 0.5% acetic acid), to control protein transfer and was destained in Tris-buffered saline (50 mM Tris-Cl, pH 7.5, 150 mM NaCl) containing 0.2% Tween-20 (TBS-T) for 5 min. Afterwards the nitrocellulose was blocked in 5% skimmed milk powder in TBS-T for 60 min, followed by a brief washing with TBS-T. Incubation with the primary antibody was done overnight under following conditions: affinity-purified polyclonal anti-TcdB IgG (in-house made [Henkel et al., 2020]) 1:1,000 in TBS-T supplemented with 5% skimmed milk powder; anti-flag-tag (Flag M2, Sigma Aldrich, Germany) 1:1,000 in TBS-T-supplemented with 5% BSA; GAPDH (Zytomed) 1:1,000 in TBS-T; β-Actin (Sigma Aldrich, Germany) 1:5,000 in TBS-T; anti-LC3B (clone D11, Cell Signaling) 1:1,000 in TBS-T; mouse monoclonal anti-LAMP1 (clone E-5, Santa Cruz, Germany) 1:200 in TBS-T; polyclonal rabbit anti-LAMP1 (Invitrogen, Germany) 1:1,000 in TBS-T.

4.9 | Statistics

All graphs show mean values with standard deviation. For significance unpaired *t*-test was performed and a *p*-value of <.05 was considered significant (*) or <.01/<.001 highly significant (**/***), respectively. All analyses were performed with GraphPad Prism 5, version 5.02, 2008.

ACKNOWLEDGMENTS

We thank the Research Core Unit for Laser Microscopy, MHH, for assistance in laser scanning microscopy. We are grateful to Monica Thelestam, Karolinska Institute, Stockholm, Sweden, for providing DonQ cells. This work was supported by the Deutsche Forschungsgemeinschaft (GE 1017/5-1 and GE 1017/6-1). This work was also supported by the Federal State Lower Saxony, Niedersächsisches Vorab (VWZN3380, Project B1). Open access funding enabled and organized by ProjektDEAL.

CONFLICT OF INTEREST

The authors declare no conflicts of interest.

AUTHOR CONTRIBUTIONS

CS, MS, HT, RG and AA conducted the experiments. MM contributed citrin-Gal3 and citrin-Gal8 transfected HEp-2 cells. RG and MM made concept for the study. RG supervised and coordinated the project. CS and MS analyzed the data. RG, CS and DH conceived and designed experiments. HT and DH generated and provided essential variant toxins. RG, CS and MM wrote the manuscript.

DATA AVAILABILITY STATEMENT

The data that support the findings of this study are available from the corresponding author upon reasonable request.

ORCID

Ralf Gerhard https://orcid.org/0000-0002-9380-3640

REFERENCES

Barth, H., Pfeifer, G., Hofmann, F., Maier, E., Benz, R. & Aktories, K. (2001) Low pH-induced formation of ion channels by *Clostridium difficile* toxin B in target cells. *Journal of Biological Chemistry*, *276*, 10670–10676. https://doi.org/10.1074/jbc.M009445200

Barth, S., Glick, D. & Macleod, K.F. (2010) Autophagy: assays and artifacts. *The Journal of Pathology*, *221*, 117–124. https://doi.org/10.1002/path.2694

Beer, L.A., Tatge, H., Reich, N., Tenspolde, M., Olling, A., Goy, S. et al. (2018a). Early cell death induced by *Clostridium difficile* TcdB: uptake and Rac1-glucosylation kinetics are decisive for cell fate. *Cellular Microbiology*, *20*, e12865.

Beer, L.A., Tatge, H., Schneider, C., Ruschig, M., Hust, M., Barton, J. et al. (2018b). The binary toxin CDT of *Clostridium difficile* as a tool for intracellular delivery of bacterial glucosyltransferase domains. *Toxins*, *10*, 225. https://doi.org/10.3390/toxins10060225

Bilverstone, T.W., Garland, M., Cave, R.J., Kelly, M.L., Tholen, M., Bouley, D.M. et al. (2020) The glucosyltransferase activity of *C. difficile* Toxin B is required for disease pathogenesis. *PLoS Pathogens*, *16*, e1008852.

Burger, S., Tatge, H., Hofmann, F., Genth, H., Just, I. & Gerhard, R. (2003) Expression of recombinant *Clostridium difficile* toxin A using the *Bacillus megaterium* system. *Biochemical and Biophysical Research Communications*, *307*, 584–588. https://doi.org/10.1016/S0006-291X(03)01234-8

Chan, H., Zhao, S., Zhang, L., Ho, J., Leung, C.C.H., Wong, W.T. et al. (2018) *Clostridium difficile* toxin B induces autophagic cell death in colonocytes. *Journal of Cellular and Molecular Medicine*, *22*, 2469–2477.

Chaves-Olarte, E., Florin, I., Boquet, P., Popoff, M., von Eichel-Streiber, C. & Thelestam, M. (1996) UDP-glucose deficiency in a mutant cell line protects against glucosyltransferase toxins from *Clostridium difficile* and *Clostridium sordellii*. *Journal of Biological Chemistry*, *271*, 6925–6932. https://doi.org/10.1074/jbc.271.12.6925

Chen, P., Tao, L., Wang, T., Zhang, J., He, A., Lam, K.H. et al. (2018) Structural basis for recognition of frizzled proteins by *Clostridium difficile* toxin B. *Science*, *360*, 664–669.

Chumbler, N.M., Farrow, M.A., Lapierre, L.A., Franklin, J.L., Haslam, D.B., Goldenring, J.R. et al. (2012) *Clostridium difficile* Toxin B causes epithelial cell necrosis through an autoprocessing-independent mechanism. *PLoS Pathogens*, *8*, e1003072.

Chung, S.Y., Schottelndreier, D., Tatge, H., Fuhner, V., Hust, M., Beer, L.A. et al. (2018) The conserved Cys-2232 in *Clostridioides difficile* Toxin B modulates receptor binding. *Frontiers in Microbiology*, *9*, 2314. https://doi.org/10.3389/fmicb.2018.02314

Egerer, M., Giesemann, T., Jank, T., Satchell, K.J. & Aktories, K. (2007) Auto-catalytic cleavage of *Clostridium difficile* toxins A and B depends on cysteine protease activity. *Journal of Biological Chemistry*, *282*, 25314–25321. https://doi.org/10.1074/jbc.M703062200

Farrow, M.A., Chumber, N.M., Bloch, S.C., King, M., Moton-Melancon, K., Shupe, J. et al. (2020) Small molecule inhibitor screen reveals calcium channel signaling as a mechanistic mediator of *Clostridium difficile* TcdB-induced necrosis. *ACS Chemical Biology*, *15*, 1212–1221.

Farrow, M.A., Chumbler, N.M., Lapierre, L.A., Franklin, J.L., Rutherford, S.A., Goldenring, J.R. et al. (2013) *Clostridium difficile* toxin B-induced necrosis is mediated by the host epithelial cell NADPH oxidase complex. *Proceedings of the National Academy of Sciences of the United States of America*, *110*, 18674–18679. https://doi.org/10.1073/pnas.1313658110

Giesemann, T., Jank, T., Gerhard, R., Maier, E., Just, I., Benz, R. et al. (2006) Cholesterol-dependent pore formation of *Clostridium difficile* toxin A. *Journal of Biological Chemistry*, *281*, 10808–10815. https://doi.org/10.1074/jbc.M512720200

Hasegawa, J., Maejima, I., Iwamoto, R. & Yoshimori, T. (2015) Selective autophagy: lysophagy. *Methods*, *75*, 128–132. https://doi.org/10.1016/j.ymeth.2014.12.014

He, R., Peng, J., Yuan, P., Yang, J., Wu, X., Wang, Y. et al. (2017) Glucosyltransferase activity of *Clostridium difficile* toxin B triggers autophagy-mediated cell growth arrest. *Scientific Reports*, *7*, 10532. https://doi.org/10.1038/s41598-017-11336-4

Henkel, D., Tatge, H., Schöttelndreier, D., Tao, L., Dong, M. & Gerhard, R. (2020) Receptor binding domains of TcdB from *Clostridioides difficile* for chondroitin sulfate proteoglycan-4 and frizzled proteins are functionally independent and additive. *Toxins*, *12*, 736. https://doi.org/10.3390/toxins12120736

Jank, T. & Aktories, K. (2008) Structure and mode of action of clostridial glucosylating toxins: the ABCD model. *Trends in Microbiology*, *16*, 222–229. https://doi.org/10.1016/j.tim.2008.01.011

Jank, T., Belyi, Y. & Aktories, K. (2015) Bacterial glycosyltransferase toxins. *Cellular Microbiology*, *17*, 1752–1765. https://doi.org/10.1111/cmi.12533

Jia, J., Bissa, B., Brecht, L., Allers, L., Choi, S.W., Gu, Y. et al. (2020) AMPK, a regulator of metabolism and autophagy, is activated by lysosomal damage via a novel galectin-directed ubiquitin signal transduction system. *Molecular Cell*, *77*, 951–969.e9. https://doi.org/10.1016/j.molcel.2019.12.028

Junemann, J., Just, I., Gerhard, R. & Pich, A. (2018) Quantitative phosphoproteome analysis of *Clostridioides difficile* toxin B treated human epithelial cells. *Frontiers in Microbiology*, *9*, 3083. https://doi.org/10.3389/fmicb.2018.03083

Just, I., Selzer, J., Wilm, M., von Eichel-Streiber, C., Mann, M. & Aktories, K. (1995) Glucosylation of Rho proteins by *Clostridium difficile* toxin B. *Nature*, *375*, 500–503. https://doi.org/10.1038/375500a0

LaFrance, M.E., Farrow, M.A., Chandrasekaran, R., Sheng, J., Rubin, D.H. & Lacy, D.B. (2015) Identification of an epithelial cell receptor responsible for *Clostridium difficile* TcdB-induced cytotoxicity. *Proceedings of the National Academy of Sciences of the United States of America*, *112*, 7073–7078.

Mizushima, N. & Yoshimori, T. (2007) How to interpret LC3 immunoblotting. *Autophagy*, *3*, 542–545. https://doi.org/10.4161/auto.4600

Orrell, K.E., Mansfield, M.J., Doxey, A.C. & Melnyk, R.A. (2020) The *C. difficile* toxin B membrane translocation machinery is an evolutionarily conserved protein delivery apparatus. *Nature Communications*, *11*, 432.

Orrell, K.E., Zhang, Z., Sugiman-Marangos, S.N. & Melnyk, R.A. (2017) *Clostridium difficile* toxins A and B: receptors, pores, and translocation into cells. *Critical Reviews in Biochemistry and Molecular Biology*, *52*, 461–473.

Ruhe, F., Olling, A., Abromeit, R., Rataj, D., Grieschat, M., Zeug, A. et al. (2017) Overexpression of the endosomal anion/proton exchanger ClC-5 increases cell susceptibility toward *Clostridium difficile* toxins TcdA and TcdB. *Frontiers in Cellular and Infection Microbiology*, *7*, 67. https://doi.org/10.3389/fcimb.2017.00067

Tao, L., Zhang, J., Meraner, P., Tovaglieri, A., Wu, X., Gerhard, R. et al. (2016) Frizzled proteins are colonic epithelial receptors for *C. difficile* toxin B. *Nature*, *538*, 350–355.

Tian, S., Liu, Y., Wu, H., Liu, H., Zeng, J.I., Choi, M.Y. et al. (2020) Genome-wide CRISPR screen identifies semaphorin 6A and 6B as receptors for *Paeniclostridium sordellii* toxin TcsL. *Cell Host and Microbe*, *27*, 782–792.e7. https://doi.org/10.1016/j.chom.2020.03.007

Wilcox, M.H., Gerding, D.N., Poxton, I.R., Kelly, C., Nathan, R., Birch, T. et al. (2017) Bezlotoxumab for prevention of recurrent *Clostridium difficile* infection. *New England Journal of Medicine*, *376*, 305–317.

Wohlan, K., Goy, S., Olling, A., Srivaratharajan, S., Tatge, H., Genth, H. et al. (2014) Pyknotic cell death induced by *Clostridium difficile* TcdB: chromatin condensation and nuclear blister are induced independently of the glucosyltransferase activity. *Cellular Microbiology*, *16*, 1678–1692.

Yuan, P., Zhang, H., Cai, C., Zhu, S., Zhou, Y., Yang, X. et al. (2015) Chondroitin sulfate proteoglycan 4 functions as the cellular receptor for *Clostridium difficile* toxin B. *Cell Research*, *25*, 157–168. https://doi.org/10.1038/cr.2014.169

Zeiser, J., Gerhard, R., Just, I. & Pich, A. (2013) Substrate specificity of clostridial glucosylating toxins and their function on colonocytes

analyzed by proteomics techniques. *Journal of Proteome Research*, *12*, 1604–1618. https://doi.org/10.1021/pr300973q

SUPPORTING INFORMATION

Additional supporting information may be found in the online version of the article at the publisher's website.

How to cite this article: Klepka, C., Sandmann, M., Tatge, H., Mangan, M., Arens, A., Henkel, D. et al. (2022) Impairment of lysosomal function by *Clostridioides difficile* TcdB. *Molecular Microbiology*, 117, 493–507. https://doi.org/10.1111/mmi.14864